

Journal of Vertebrate Paleontology



ISSN: (Print) (Online) Journal homepage: https://www.tandfonline.com/loi/ujvp20

Quantifying vascularity in the frontoparietal dome of *Stegoceras validum* (Dinosauria: Pachycephalosauridae) from high resolution CT scans

Jasmine A. Nirody, Mark B. Goodwin, John R. Horner, Tony L. Huynh, Matthew W. Colbert, David K. Smith & David C. Evans

To cite this article: Jasmine A. Nirody, Mark B. Goodwin, John R. Horner, Tony L. Huynh, Matthew W. Colbert, David K. Smith & David C. Evans (2022) Quantifying vascularity in the frontoparietal dome of *Stegoceras validum* (Dinosauria: Pachycephalosauridae) from high resolution CT scans, Journal of Vertebrate Paleontology, 41:5, e2036991, DOI: 10.1080/02724634.2021.2036991

To link to this article: https://doi.org/10.1080/02724634.2021.2036991

	Published online: 17 Mar 2022.
	Submit your article to this journal $oldsymbol{\mathcal{C}}$
ılıl	Article views: 281
α̈́	View related articles 🗹
CrossMark	View Crossmark data ☑



ARTICLE

QUANTIFYING VASCULARITY IN THE FRONTOPARIETAL DOME OF *STEGOCERAS VALIDUM* (DINOSAURIA: PACHYCEPHALOSAURIDAE) FROM HIGH RESOLUTION CT SCANS

JASMINE A. NIRODY, $^{\bullet}*,^{1,2}$ MARK B. GOODWIN, JOHN R. HORNER, $^{\bullet}4$ TONY L. HUYNH, MATTHEW W. COLBERT, DAVID K. SMITH, and DAVID C. EVANS^{8,9}

¹All Souls College, University of Oxford, Oxford OX1 4AL, U.K., jasmine.nirody@all-souls.ox.ac.uk;
²Center for Studies in Physics and Biology, Rockefeller University, New York, New York 10021 U.S.A., jnirody@rockefeller.edu;
³Museum of Paleontology, University of California, 1101 Valley Life Sciences Building, Berkeley, California 94720 U.S.A., mark@berkeley.edu;

⁴Chapman University, One University Drive, Orange, California 92866 U.S.A., jhorner@chapman.edu; ⁵Museum of Paleontology, University of California, 1101 Valley Life Sciences Building, Berkeley, California 94720 U.S.A., huyntony@berkeley.edu;

⁶High-Resolution X-ray CT Facility, Jackson School of Geosciences, University of Texas at Austin, C1100, Austin, Texas 78712 U.S.A., colbert@utexas.edu;

⁷Museum of Paleontology, University of California, 1101 Valley Life Sciences Building, Berkeley, California 94720 U.S.A., httms@berkeley.edu:

⁸Royal Ontario Museum, 100 Queens Park, Toronto, Ontario M5S 2C6, Canada, d.evans@utoronto.ca;

⁹Department of Ecology and Evolutionary Biology, University of Toronto, 25 Willcocks Street, Toronto, Ontario M5S 3B2, Canada;

ABSTRACT—The thickened frontoparietal in pachycephalosaurid dinosaurs expands dramatically during ontogeny from a flat-headed to a domed state. This expansion results in the formation of zonal tissue characterized largely by differences in vascularity and bony tissue structure that changes through ontogeny. Void space identified in CT scans of the frontoparietal is a suitable proxy for relative vascularity. An increase in relative vascularity occurs with the development of the dome in the pachycephalosaur *Stegoceras validum*, followed by a significant decrease in late stage ontogeny. We employ a script adapted from an algorithm for human cortical bone imaging to: (1) determine the percent vascularity in any given CT slice; (2) quantify these observed changes in relative vascularity within a complete frontoparietal; and (3) identify ontogenetic changes in vascularity from a cranial growth series of *Stegoceras*. Morphological landmarks identified in the CT scans facilitate an accurate slice-by-slice comparison of homologous regions of the dome between skulls. This new tool enables: (1) a complete assessment of bone vascularity from CT scans; (2) is applicable to any fossil or modern bone in the vertebrate skeleton; and (3) provides an alternative measure to pixel-by-pixel manual thresholding, a time intensive and subjective process.

Citation for this article: Nirody, J.A., M. B. Goodwin, J. R. Horner, T. L. Huynh, M. W. Colbert, D. K. Smith, and D. C. Evans. 2022. Quantifying vascularity in the frontoparietal dome of *Stegoceras validum* (Dinosauria: Pachycephalosauridae) from high resolution CT scans. Journal of Vertebrate Paleontology. DOI: 10.1080/02724634.2021.2036991

INTRODUCTION

Pachycephalosaurid dinosaurs are a clade of small-to-medium sized bipedal herbivores characterized by a thickened skull roof and inflation of the frontals and parietal into a cranial dome (Maryańska et al., 2004). The frontals and parietal expand dramatically during ontogeny from a flat-headed into a domed state via formation of zonal bone tissue that has been subdivided internally into three zones characterized by differences in porosity or vascularity (see Goodwin and Horner, 2004). An increase in relative vascularity correlates with the early development of the frontoparietal dome in *Stegoceras validum* during ontogeny (Goodwin and Horner, 2004).

Schott et al. (2011) were the first to use HRCT scan slices to quantify bone histological signals in pachycephalosaurids using the Huang thresholding method. Due to the complexity of using a full CT dataset, a homologous slice of the frontal at the

*Corresponding author

contact of the posterior supraorbital and postorbital sutures was used as a proxy to compare vascularity. Schott et al. (2011) noted a decreasing trend in vascularity through a hypothesized ontogenetic series of cranial domes in *Stegoceras validum*. Subsequent studies employed this method to quantify and assess ontogenetic patterns in the dome of other pachycephalosaurids including *Foraminacephale brevis* (Schott and Evans, 2017) and *Sphaerotholus buchholtzae* (Woodruff et al., 2021), and found the same general trend.

Bone porosity, identified in CT scans as void space, has been used as a proxy for vascularity in pachycephalosaurs (Schott et al., 2009; Schott and Evans, 2017; Woodruff et al., 2021). Relative bone porosity is also recorded as percent vascularity or vascular density (Lee et al., 2013 and references cited therein). We use the term 'percent vascularity' in this study, following previous work, while recognizing that these spaces also contain nervous tissue as part of the neurovascular network, lymphatics, and connective tissues in vivo (e.g., Starck and Chinsamy, 2002). Percent vascularity is useful as an alternative measure of vascular canal size and distribution throughout bone tissue. This calculation is

important because: (1) relative porosity describes irregularly shaped canals within a three-dimensional bone matrix with a single value; (2) growth rate is associated with cortical bone porosity in vertebrates (Williams et al., 2004); and (3) in cortical, and by inference dermal bone, faster-growing individuals of the same age possess significantly more porous bone tissue (Lee et al., 2013).

Here, we present a script written in MATLAB adapted from an algorithm for human cortical bone imaging (Kazakia et al., 2014; Nirody et al., 2015) to quantify patterns of vascularity of the frontoparietal and measure how it compares across the expanding dome. Morphological landmarks enable a homologous slice-by-slice comparison between skulls. This algorithm is an ideal method to evaluate variation in vascularity in other bones, modern or fossil, in the vertebrate skeleton.

Institutional Abbreviations—AMNH, American Museum of Natural History, New York, U.S.A.; TMP, Royal Tyrrell Museum of Palaeontology, Drumheller, Alberta, Canada; UALVP, University of Alberta Laboratory for Vertebrate Paleontology, Edmonton, Canada; UCMP, University of California Museum of Paleontology, Berkeley, U.S.A.; UTCT, University of Texas High Resolution X-Ray CT Facility, Austin, U.S.A.

MATERIALS AND METHODS

An assemblage of three specimens assigned to the genus *Stegoceras* (Fig. 1) represent a hypothetical cranial growth series spanning flat-headed to fully domed states. The three skulls are from relatively close proximity in space and time, the Campanian Stage of Alberta and Montana, and are from closely related species. Dinosaur cranial growth is a continuum and the terms juvenile, subadult, and adult are based on comparative cranial morphology and histological details revealed in the CT slices. Cranial growth patterns are likely conserved in *Stegoceras* and closely related pachycephalosaurid taxa (Williamson and Carr, 2002; Schott et al., 2011). Detailed locality information is available to qualified researchers from the repository of record.

AMNH 5450 is the youngest ontogimorph of *S. validum* in the growth series and was collected by Barnum Brown in 1913 from the Dinosaur Park Formation, Alberta, Canada in the valley of the Red Deer River, 1 mile below Steveville. Historically referred to as "primitive" due to the lack of a dome and large supratemporal fenestrae (Wall and Galton, 1979), AMNH 5450 represents an early juvenile stage of *S. validum* with flat, thickened frontals and parietal (Goodwin et al., 1998; Williamson and Carr, 2002; Schott et al., 2011).

TMP 1984.005.0001 is a partial skull of *S. validum* from the Upper Cretaceous lower Oldman Formation, Steveville area, Alberta, Canada. A subadult age assignment is supported by the domed frontals paired with an uninflated parietal, open supratemporal fenestrae, dorsal tubercular ornamentation, and open cranial sutures (Schott et al., 2011).

UCMP 130051 is a fully domed adult skull and the most complete *Stegoceras*-grade pachycephalosaurid skull from the Judith River Formation, Hill County, Montana. It has been identified previously as *Stegoceras* sp. (Williamson and Carr, 2002) or *Hanssuesia sternbergi* (Sullivan, 2003), or alternatively it may represent a distinct species. UCMP 130051 was used as a hypothetical end member of a *Stegoceras validum* cranial growth series in other studies (Williamson and Carr, 2002). UCMP 130051 possesses a smooth dorsal surface, reduced cranial ornamentation, closed supratemporal fenestrae, and extremely low vascularity throughout the nearly solid frontoparietal dome. Midline frontal and frontoparietal suture obliteration are extreme and contrasts with the open lateral cranial sutures.

High Resolution CT Imaging

The frontoparietal in TMP 1984.005.0001 and UCMP 130051 was segmented out digitally from the CT scans prior to analysis by the MATLAB script to account for preservational differences in the sample set. Note that optimal scanning resolution requires voxels in the 40–80 micron range for the analysis presented here. Scans may be adequate to image sutures and bone texture, but fail to binarize due to limited scan resolution. The resolution of CT scans completed at UTCT in 2000 of the iconic young adult skull of *Stegoceras validum*, UAVLP 2 (see Bourke et al. 2014), was insufficient for our analysis. As a result, UCMP 130051 was selected as the adult end member.

Scan parameters and associated metadata were archived on MorphoSource.org: https://doi.org/10.17602/M2/M397335 [AMNH 5450 frontoparietal]; https://doi.org/10.17602/M2/M397362 [TMP 1984.005.0001 partial skull; frontoparietal];

https://doi.org/10.17602/M2/M397324 [UCMP 130051 partial skull; frontoparietal].

Image Segmentation and Quantification of Porosity Metrics

MATLAB Script—Image analysis was performed in MATLAB (The MathWorks, Inc., Natick, MA, USA). A freely available Python version of the same analysis workflow was also made available. Image stacks were read in slice-by-slice and were registered using an automated intensity-based method. For each slice, a fixed-threshold binarization was applied to the grayscale image using Otsu's method, which separates pixels in the image into two classes using a single intensity threshold chosen to maximize the variance between foreground and background pixels (Otsu, 1979). Void space threshold was set for a random slice from each individual specimen. The grayscale range for the void space will vary between specimens since fossils scan differently due to preservational variances. All successive analysis and quantification were performed using the resulting binary images.

To account for artifacts or surface roughness and ensure the full sample was included, a morphological closing of the image was implemented to connect erroneously separated regions (Kazakia et al., 2014). After this, contours delineating the perimeter of the bone were drawn. Qualitative inspection of the automated generated contours was performed for quality assurance. If a contour visibly deviated from the apparent boundary, minor adjustments were made manually to the affected region, leaving the remainder of the contour unaffected. The total area within a slice was calculated using all pixels within this perimeter.

Within each layer, percent vascularity was computed to quantify regional porosity. These vascular spaces also contain nervous tissue as part of the neurovascular network and lymphatics *in vivo* (e.g., Starck and Chinsamy, 2002). These additional structures require standard histological techniques and microCT synchrotron analysis to image in fossils (Horner et al., 2014) and are not under consideration in this study.

Pore pixels were summed at each slice to generate a per-slice total pore area; per-slice percent vascularity was then calculated from this value by division with the total slice area (calculated as the sum of pixels in the filled, closed image; see Fig. 2). Individual pore areas were also stored for each slice providing a method to compute the mean and variance of the pore size distribution if desired. Total percent vascularity for the entire sample was then calculated as means across all slices of per-slice percent vascularity. Samples were normalized by dividing by the total number of slices, allowing comparison of samples with differing thicknesses. Morphological landmarks used were the ventral contact of the frontonasal suture at the anterior end of the frontoparietal dome and the posteriormost ventral terminus of the parietal (see Goodwin, 1990; Schott et al., 2011). Additional

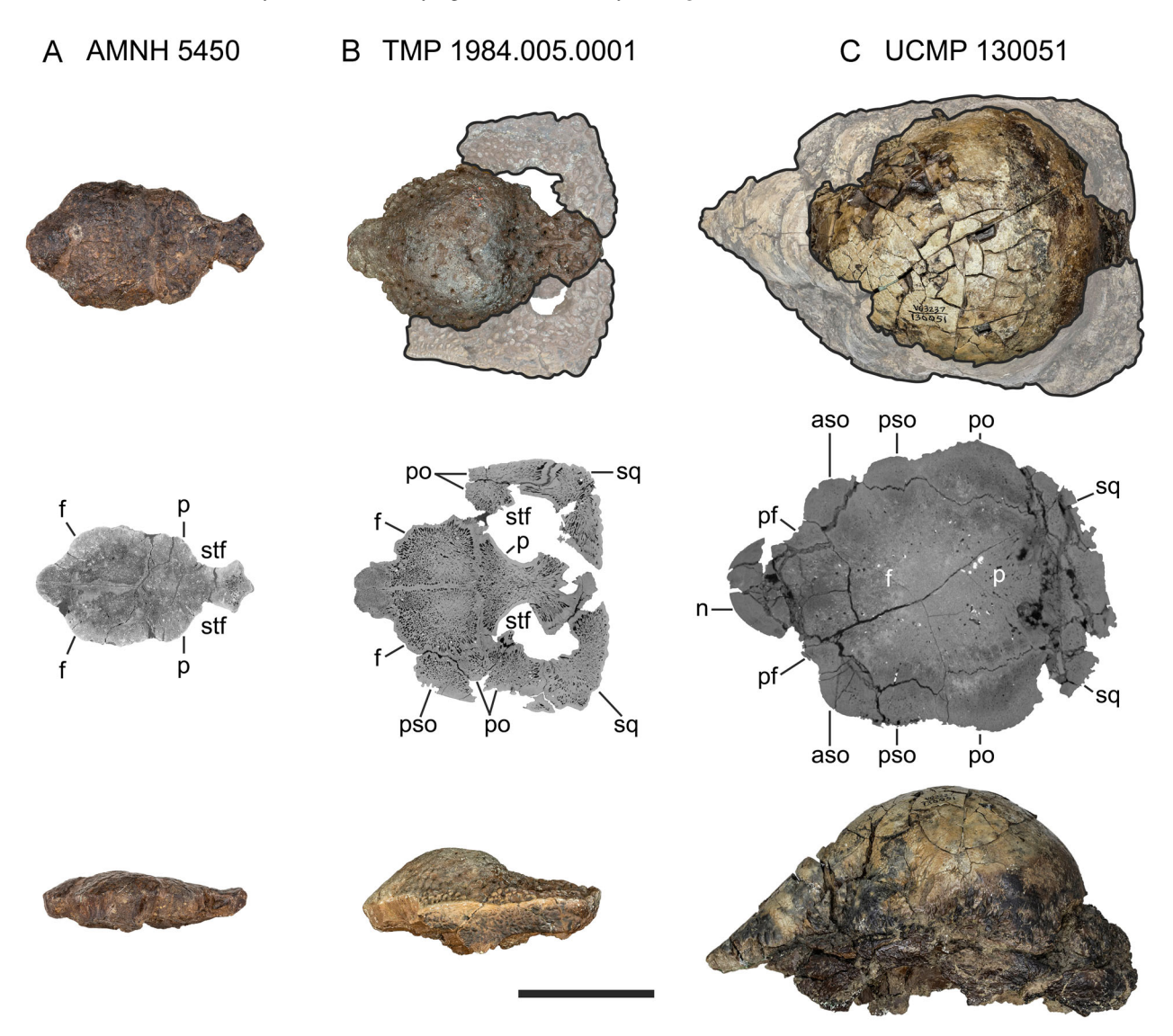


FIGURE 1. Growth series of *Stegoceras validum* in dorsal (top, middle) and left lateral (bottom) views. CT slices in the middle row reveal cranial sutures and contrasting tissue texture in the development of the frontoparietal from a flat-headed to a domed morphology. **A**, AMNH 5450, holotype of *Ornatotholus browni* now recognized as the frontoparietal of a juvenile *S. validum*; **B**, TMP 1984.005.0001, a subadult partial skull of *S. validum*; **C**, UCMP 130051, a partial skull of *S. validum* (or possibly a new species of *Stegoceras*-grade pachycephalosaur) represents an adult. The shaded areas in B and C (top row) were excluded from the MATLAB script analysis to ensure equivalent comparisons of relative vascularity in the frontal + parietal (= frontoparietal) only. **Abbreviations: aso**, anterior supraorbital; **f**, frontal; **n**, nasal; **p**, parietal; **pf**, prefrontal; **po**, postorbital; **pso**, posterior supraorbital; **sq**, squamosal; **stf**, supratemporal fenestra. Scale bar equals 5 cm.

landmarks, such as the frontoparietal suture, were identified in individual CT slices and facilitated comparisons between specimens. All code is available at https://github.com/jnirody/domeporosity.

RESULTS

The combined bivariate plot of percent vascularity is normalized and provides a slice-by-slice comparison of the three specimens of *Stegoceras validum* (Fig. 3). AMNH 5450 records a mean vascularity of 14.5% and vascularity is relatively constant throughout the frontoparietal at this early ontogenetic stage. This compares reasonably well to the 20.1% vascularity reported for the same specimen in the single slice approach of Schott et al. (2011).

The frontals reveal initial doming reflected in the slightly higher percent vascularity compared with the thickened parietal

which inflates after the frontals. The posterior parietal has a pronounced increase in percent vascularity prior to expansion of the dome in both AMNH 5450 and TMP 1984.005.0001. TMP 1984.005.0001 records a mean vascularity of 28.0% in this study, compared with 17% in Schott et al. (2011). This relatively greater percent vascularity stems from an inflated frontal, partially inflated parietal, and the older ontogenetic age of TMP 1984.005.0001 compared with AMNH 5450. UCMP 130051 is the oldest ontogenetically in the growth series and is characterized by a significant decrease in vascularity throughout the entire frontoparietal dome that is nearly solid comparatively with a mean vascularity of 1.2%. This trend in relative vascularity of the frontoparietal in Stegoceras agrees with the observations proposed earlier by Goodwin and Horner (2004), but differs from that in Schott et al. (2011), in which vascularity was observed to decrease from flat-headed to fully domed state, a

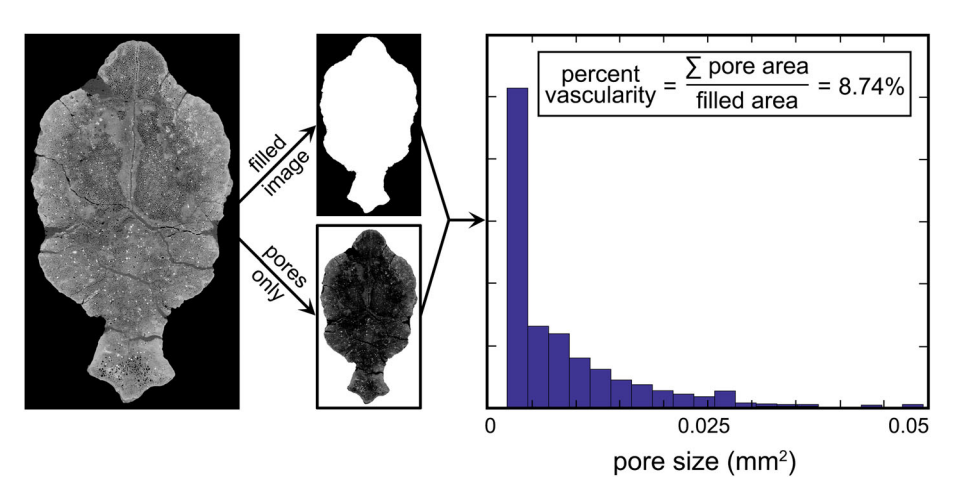


FIGURE 2. An overview of the segmentation algorithm and porosity quantification workflow. The original grayscale CT image of the frontoparietal of Stegoceras validum, AMNH 5450, is binarized using a global threshold determined by Otsu's method (Otsu, 1979). This binarized image is separated into an image denoting the filled area of the bone and an image marking only the pores within the bone. The porosity of a slice (percent vascularity) is defined as the sum of the area of each pore divided by the total filled area of the bone. In addition to global statistics, our proposed workflow computes the entire distribution of pore area and localization which allows for more detailed analysis. The field of bright spots is an artifact from the charging of mineral infilling during CT scanning.

pattern almost certainly due to the more limited single slice focus of their analysis.

In the juvenile and subadult stages of AMNH 5450 and TMP 1984.005.0001 respectively, two zones of expansion (or developing expansion) are identified by increasing vascularity of the frontals (~0-0.5 on the X axis) and parietal (~0.5-1.0 on the X axis) in Fig. 3. The location of the frontal-parietal suture is indicated by a slight decrease in vascularity, a result of denser bone in the area of sutural contact at 0.5 in AMNH 5450 and TMP 1984.005.0001 (shaded bars in Fig. 3). UCMP 130051 does not exhibit an equivalent decrease in vascularity at the frontal-parietal suture loci on account of frontal-parietal suture obliteration and more uniform, low porosity.

The frontal-parietal suture is visible in slice no. 870 in TMP 1984.005.0001 in coronal view and indicated on the bivariate plot by the black vertical line (Fig. 4). Three zones of growth are revealed in slice no. 870 and confirm the contrasting porosity and density between the frontal-parietal suture and the surrounding tissue. This slice-by-slice plot of percent vascularity demonstrates the variability within the frontoparietal dome.

DISCUSSION

Degree of porosity, microstructure, and comparative histology are used to analyze and infer dynamic processes in both modern (e.g., Bouxsein et al., 2010 and references therein) and fossil bone (e.g., Huttenlocker et al., 2013 and references therein) and to document patterns of suture morphology and variation (Bailleul and Horner, 2016; Bailleul et al., 2016). Bone tissue vascularity in extinct animals is useful in characterizing the evolution and development of novel cranial anatomical features in deep time (e.g., Kulik and Sidor, 2019; Nesbitt et al., 2021). Similarly, the analysis and characterization of phenotypic specializations in bone shape and density, cortical thickness, and vascularity in extant species have proven helpful in forming and testing various ecomorphological and phylogenetic hypotheses (e.g., Samuels and Van Valkenburgh, 2008; Doube et al., 2009; Houssaye et al., 2016; Kilbourne and Hutchinson, 2019).

Early studies showed that bone porosity is not spatially uniform (Atkinson, 1965). Importantly, regional analysis—that is, analysis of the distribution of porosity rather than simply averaged metrics—has also shown to have functional relevance for

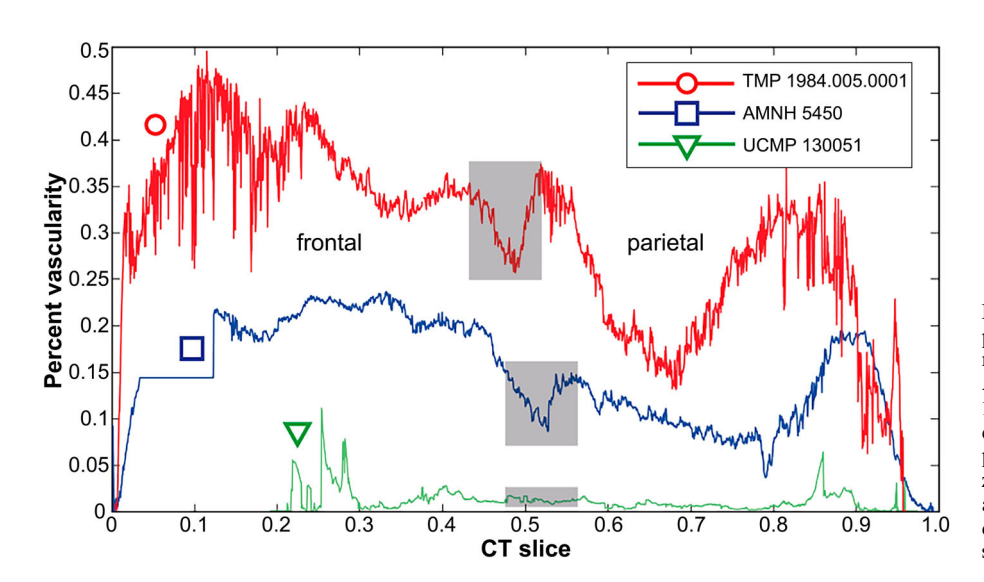
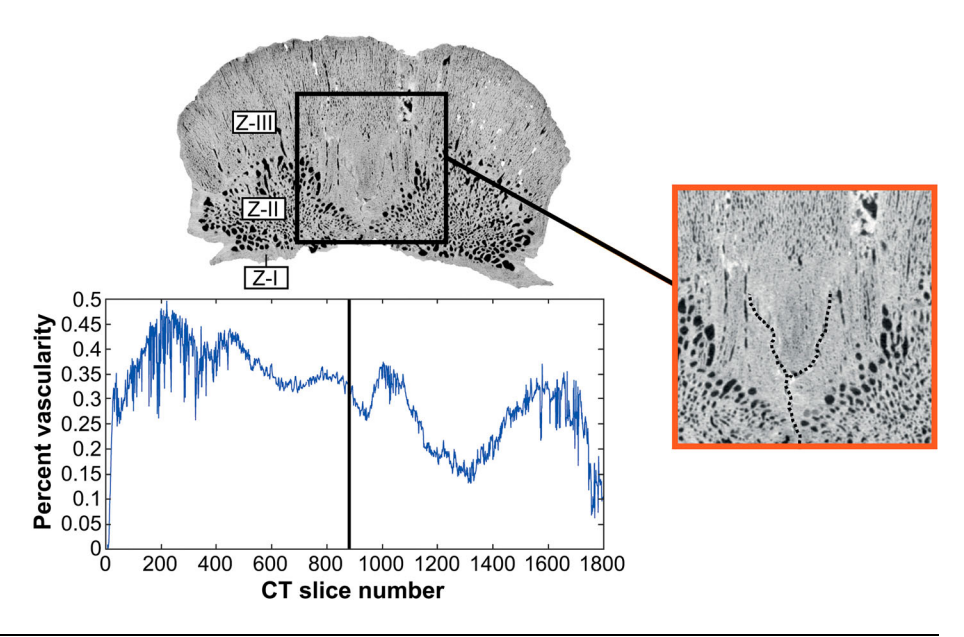


FIGURE 3. Slice-by-slice normalized plot of percent vascularity in three *Stegoceras* specimens. The mean percent vascularity of AMNH 5450 equals 14.5%, TMP 1984.005.0001 mean percent vascularity equals 28.0%, and UCMP 130051 mean percent vascularity equals 1.2%. A separate zone of expansion occurs in the paired frontals and parietal in the juvenile and subadult domes. The location of the frontoparietal suture is indicated by the shaded bars.

FIGURE 4. Percent vascularity (PV) versus CT slice number for the frontoparietal dome of TMP 1984.005.0001. Three zones of dome growth (sensu Goodwin and Horner, 2004) are labeled Z-I, Z-II, and Z-III. Denser bone appears lighter-colored in the CT slice. The black vertical line marks the position of slice no. 870 shown above the graph. Percent vascularity continues to decrease slightly along the denser frontoparietal sutural contact at slice no. 870, peaks at slice no. 1000, before decreasing again at slice no. 1300. A final increase in PV occurs prior to inflation of the parietal into the dome. The frontal-parietal sutural contact appears as a distinctive "V"-shape internally where the anterior projection of the parietal bisects the left and right frontals. The frontal-parietal suture is traced by the black dotted line in the enlarged call-out.



locomotor performance (e.g., Skedros et al., 2004; Atkins et al., 2014), as well as to elucidate the mechanisms underlying age-, gender-, or species-related variation in bone microstructure (e.g., Kazakia et al., 2014; Wang et al., 2020). For example, quantification of pore distributions and the associated longitudinal changes in these distributions may provide insight into pore network expansion (e.g., Nirody et al., 2015; Heilmeier et al., 2016). Determining microstructure distribution may also prove helpful in assessing fracture risk and providing personalized pharmacologic interventions. However, the lack of automated workflows has limited the widespread use of distribution analysis thus far.

We demonstrate that cranial vascularity varies throughout the rapidly growing frontoparietal dome by evaluating both individual CT slices and the total range of values present in the entire specimen. This approach improves upon the single slice analysis by Schott et al. (2011) because use of a single slice approach fails to capture this variation. This can lead to mischaracterization of dome growth due to variable timing of dome expansion and individual variation. The 3D thresholding and visualization approach taken here provide a more complete characterization of the vascular patterns in bone and a more data-rich approach to ontogenetic studies of bone dynamics.

CONCLUSION

Here, we present a script for semi-automated quantification of both percent vascularity as well as pore size and spatial distribution in any bone or biomineralized tissue. The script offers a repeatable, standardized alternative to manual thresholding and segmentation. We provide both MATLAB and Python scripts that implement the method described (available at https://github.com/jnirody/domeporosity), in complement to available ImageJ macros (Doube et al., 2010). Importantly, the modular nature of our workflow allows for easy customization by users. Comparisons are improved when morphological landmarks, such as sutures or tissue regions, are identified in CT scans. This script: (1) facilitates the documentation of vascularity, sutural morphology, tissue texture, and growth patterns in modern and fossil bone; (2) complements 2D histological studies; and (3) has potentially broader application in vertebrate

paleontology and paleobiology beyond the study of dinosaurs as well as human and veterinary medicine.

ACKNOWLEDGMENTS

The National Science Foundation grants EAR-1053370 to M.B.G. and EAR-1561622 to UTCT provided financial support for this research. The Doris O. and Samuel P. Welles Fund and the UCMP contributed funding and facilities support to M.B.G. This research was also supported by an NSERC Discovery Grant (File Number: RGPIN-2018-06788) to D.C.E. Funding for uploading the CT data to MorphoSource was provided by NSF grant DBI-1902242 to J. Maisano and D. Blackburn. Discussions with C. Marshall, P. Holroyd, and R. Full were beneficial. P. Currie granted access to the CT scans of UAVLP 2. D. Strauss provided photographs of AMNH 5450, TMP 1984.005.0001, and UCMP 130051. W. Dunaway assisted with computer and software support. L. Weaver and an anonymous reviewer reviewed an earlier draft of this article; M. D'Emic provided editorial guidance, and we thank all of them for their useful comments and suggestions. We thank C. Mehling (AMNH) and B. Strilisky (TMP) for facilitating loans of AMNH 5450 and TMP 1984.005.0001 respectively. This is University of California Museum of Paleontology contribution 3011.

ORCID

Jasmine A. Nirody http://orcid.org/0000-0002-0461-1031 John R. Horner http://orcid.org/0000-0003-1806-1656

LITERATURE CITED

Atkins, A., M. N. Dean, M. L. Habegger, P. J. Motta, L. Ofer, F. Repp, A. Shipov, S. Weiner, J. D. Currey, and R. Shahar. 2014. Remodeling in bone without osteocytes: billfish challenge bone structure–function paradigms. Proceedings of the National Academy of Sciences 111:16047–16052.

Atkinson, P. J. 1965. Changes in resorption spaces in femoral cortical bone with age. Journal of pathology and bacteriology 89:173–178.
 Bailleul, A. M., and J. R. Horner. 2016. Comparative histology of some craniofacial sutures and skull-base synchondroses in non-avian

- dinosaurs and their extant phylogenetic bracket. Journal of Anatomy 229:252–285.
- Bailleul, A. M., J. B. Scannella, J. R. Horner, and D. C. Evans. 2016. Fusion patterns in the skulls of modern archosaurs reveal that sutures are ambiguous maturity indicators for the Dinosauria. PLoS ONE 11:e0147687.
- Bourke, J. M., P. W. M. Ruger, R. C. Ridgely, T. R. Lyson, E. R. Schachner, P. R. Bell, and L. M. Witmer. 2014. Breathing life into dinosaurs: tackling challenges of soft-tissue restoration and nasal airflow in extinct species. The Anatomical Record 297:2148–2186.
- Bouxsein, M. L., S. K. Boyd, B. A. Christiansen, R. E. Guldberg, K. J. Jepsen, and R. Müller. 2010. Guidelines for assessment of bone microstructure in rodents using micro-computed tomography. Journal of Bone and Mineral Research 7:1468–1486.
- Doube, M., A. W. Conroy, P. Christiansen, J. R. Hutchinson, and S. Shefelbine. 2009. Three-dimensional geometric analysis of felid limb bone allometry. PLoS One 4:e4742.
- Doube, M., M. M. Kłosowski, I. Arganda-Carreras, F. P. Cordelières, R. P. Dougherty, J. S. Jackson, B. Schmid, J. R. Hutchinson, and S. J. Shefelbine. 2010. BoneJ: free and extensible bone image analysis in ImageJ. Bone 47:1076–1079.
- Goodwin, M. B., 1990. Morphometric landmarks of pachycephalosaurid cranial material from the Judith River Formation of northcentral Montana; pp. 189–201 in K. Carpenter and P. J. Currie (eds.), Dinosaur Systematics—Approaches and Perspectives. Cambridge University Press, Cambridge, United Kingdom.
- Goodwin, M. B., E. A. Buchholtz, and R. E. Johnson. 1998. Cranial anatomy and diagnosis of *Stygimoloch spinifer* (Ornithischia: Pachycephalosauria) with comments on cranial display structures in agonistic behavior. Journal of Vertebrate Paleontology 18:363–375.
- Goodwin, M. B., and J. R. Horner. 2004. Cranial histology of pachycephalosaurs (Ornithischia:Marginocephalia) reveals transitory structures inconsistent with head-butting behavior. Paleobiology 30:253–267.
- Heilmeier, U., K. Cheng, C. Pasco, R. Parrish, J. Nirody J. M. Patsch, C. A. Zhang, G. B. Joseph, A. J. Burghardt, A. V. Schwartz, T. M. Link, and G. Kazakia. 2016. Cortical bone laminar analysis reveals increased midcortical and periosteal porosity in type 2 diabetic postmenopausal women with a history of fragility fractures compared to fracture-free diabetics. Osteoporosis International 27:2791–2802.
- Horner, J. R., M. B. Goodwin, and V. S. Weaver. 2014. Nerve-like structures in the enigmatic domes of pachycephalosaurids. Journal of Vertebrate Paleontology Program and Abstracts 74th Annual Meeting of the Society of Vertebrate Paleontology, Berlin, p.150.
- Houssaye, A., P. M. Sander, and N. Klein. 2016. Adaptive patterns in aquatic amniote bone microanatomy–more complex than previously thought. Integrative and Comparative Biology 56:1349–1369.
- Huttenlocker, A. K., H. N. Woodward, and B. K. Hall. 2013. The Biology of Bone; pp. 13–34 in K. Padian and E.-T. Lamm (eds.), Bone histology of fossil tetrapods. University of California Press, Berkeley, California.
- Kazakia, G. J., W. Tjong, J. A. Nirody, A. J. Burghardt, J. Carballido-Gamio, J. M. Patsch, T. M. Link, B. T. Feeley, and C. B. Ma. 2014. The influence of disuse on bone microstructure and mechanics assessed by HR-pQCT. Bone 63:132–140.
- Kilbourne, B. M., and J. R. Hutchinson. 2019. Morphological diversification of biomechanical traits: mustelid locomotor specializations and the macroevolution of long bone cross-sectional morphology. BMC Evolutionary Biology 19:1–16.
- Kulik Z. T., and C. A. Sidor. 2019. The original boneheads: histologic analysis of the pachyostotic skull roof in Permian burnetiamorphs (Therapsida; Biarmosuchia). Journal of Anatomy 235:151–166.
- Lee, A. H., A. K. Huttenlocker, K. Padian, and H. N. Woodward. 2013. Analysis of Growth Rates; pp. 217–251 in K. Padian and E.-T.

- Lamm (eds.), Bone histology of fossil tetrapods. University of California Press, Berkeley, California.
- Maryańska, T., R. E. Chapman, and D. B. Weishampel. 2004. Pachycephalosauria; pp. 464–477 in D. B. Weishampel, P. Dodson, and H. Osmólska (eds.), The Dinosauria 2nd ed. University of California Press, Berkeley, California.
- Nesbitt, S. J., M. R. Stocker, S. Chatterjee, J. R. Horner, and M. B. Goodwin. 2021. A remarkable group of thick-headed Triassic period archosauromorphs with a wide, possible Pangean distribution. Journal of Anatomy 239:1–24.
- Nirody, J. A., K. P. Cheng, R. M. Parrish, A. J. Burghardt, S. Majumdar, T. M. Link, and G. J. Kazakia. 2015. Spatial distribution of intracortical porosity varies across age and sex. Bone 75:88–95.
- Otsu, N. 1979. A threshold selection method from gray-level histograms. IEEE Transactions on Systems, Man, and Cybernetics 9:62–66.
- Samuels, J. X., and B. Van Valkenburgh. 2008. Skeletal indicators of locomotor adaptations in living and extinct rodents. Journal of Morphology 269:1387–1411.
- Schott, R. K., and D. C. Evans. 2017. Cranial variation and systematics of Foraminacephale brevis gen. nov. and the diversity of pachycephalosaurid dinosaurs (Ornithischia: Cerapoda) in the Belly River Group of Alberta, Canada. Zoological Journal of the Linnean Society 179:865–906.
- Schott, R. K., D. C. Evans, M. B. Goodwin, C. B. Brown, J. R. Horner, and N. R. Longrich. 2009. The anatomy and systematics of *Colepiocephale lambei* (Dinosauria: Pachycephalosauridae). Journal of Vertebrate Paleontology 29:771–786.
- Schott, R. K, D. C. Evans, M. B. Goodwin, J. R. Horner, C. M. Brown, and N. R. Longrich. 2011. Cranial ontogeny in *Stegoceras validum* (Dinosauria: Pachycephalosauria): A quantitative model of pachycephalosaur dome growth and variation. PLoS One 6:e21092.
- Skedros, J. G., K. J. Hunt, and R. D. Bloebaum. 2004. Relationships of loading history and structural and material characteristics of bone: development of the mule deer calcaneus. Journal of Morphology 3:281–307.
- Starck, J. M., and A. Chinsamy. 2002. Bone microstructure and developmental plasticity in birds and other dinosaurs. Journal of Morphology 254:232–246.
- Morphology 254:232–246.

 Sullivan, R. M. 2003. Revision of the dinosaur *Stegoceras lambe* (Ornithischia, Pachycephalosauridae). Journal of Vertebrate Paleontology 23:181–207.
- Wall, W. P., and P. M. Galton. 1979. Notes on pachycephalosaurid dinosaurs (Reptilia: Ornithischia) from North America, with comments on their status as ornithopods. Canadian Journal of Earth Sciences 16:1176–1186.
- Wang, M., J. K. O'Connor, A. M. Bailleul, and Z. Li. 2020. Evolution and distribution of medullary bone: evidence from a new Early Cretaceous enantiornithine bird. National Science Review 7:1068– 1078
- Williams, B. D. Waddington, D. H. Murray, and C. Farquarson. 2004. Bone strength during growth: influence of growth rate on cortical porosity and mineralization. Calcified Tissue International 74:236–245.
- Williamson, T. E., and T. D. Carr. 2002. A new genus of derived pachycephalosaurian from western North America. Journal of Vertebrate Paleontology 22:779–801.
- Woodruff, D. C., M. B. Goodwin, T. R. Lyson, and D. C. Evans. 2021. Ontogeny and variation of the pachycephalosaurine dinosaur *Sphaerotholus buchholtzae*, and its systematics within the genus. Zoological Journal of the Linnean Society 193:563–601.

Submitted June 9, 2021; revisions received January 7, 2022; accepted January 10, 2022.

Handling Editor: Michael D'Emic.